Construction of AlGaN/GaN high-electron-mobility transistor-based biosensor for ultrasensitive detection of SARS-CoV-2 spike proteins and virions

Yang, Chenyang ; Sun, Jianwen; Zhang, Yulong; Tang, Jingya ; Liu, Zizheng; Zhan, Teng; Wang, Dian-Bing ; Zhang, Guoqi ; Liu, Zewen; Zhang, Xian-En

Important note
To cite this publication, please use the final published version (if applicable).
Please check the document version above.

Construction of AlGaN/GaN high-electron-mobility transistor-based biosensor for ultrasensitive detection of SARS-CoV-2 spike proteins and virions

Chenyang Yang [a,f,1], Jianwen Sun [b,1], Yulong Zhang [b], Jingya Tang [a,f], Zizheng Liu [a], Teng Zhan [e], Dian-Bing Wang [a,**], Guoqi Zhang [d,***], Zewen Liu [b,****], Xian-En Zhang [a,c,f,*]

[a] *Key Laboratory of Biomacromolecules (CAS), National Laboratory of Biomacromolecules, CAS Center for Excellence in Biomacromolecules, Institute of Biophysics, Chinese Academy of Sciences, Beijing, 100101, China*
[b] *School of Integrated Circuits, Tsinghua University, Beijing, 10084, China*
[c] *Faculty of Synthetic Biology, Shenzhen Institute of Advances Technology, Shenzhen, 518055, China*
[d] *Department of Microelectronics, Delft University of Technology, 2628, CD Delft, the Netherlands*
[e] *Research and Development Center for Solid State Lighting, Institute of Semiconductors, Chinese Academy of Sciences, Qinghua East Road 35A, Beijing, 10083, China*
[f] *University of Chinese Academy of Science, Beijing, 100049, China*

A B S T R A C T

The COVID-19 pandemic has highlighted the need for rapid and sensitive detection of SARS-CoV-2. Here, we report an ultrasensitive SARS-CoV-2 immunosensor by integration of an AlGaN/GaN high-electron-mobility transistor (HEMT) and anti-SARS-CoV-2 spike protein antibody. The AlGaN/GaN HEMT immunosensor has demonstrated the capability to detect SARS-CoV-2 spike proteins at an impressively low concentration of 10^{-22} M. The sensor was also applied to pseudoviruses and SARS-CoV-2 ΔN virions that display the Spike proteins with a single virion particle sensitivity. These features validate the potential of AlGaN/GaN HEMT biosensors for point of care tests targeting SARS-CoV-2. This research not only provides the first HEMT biosensing platform for ultrasensitive and label-free detection of SARS-CoV-2.

1. Introduction

COVID-19 has caused unparalleled damage to the public health and global economy. Though many countries have functionally declared the end to the pandemic, its scattered occurrence and recurrence remain to be the long-term threat. Therefore, precise and rapid diagnoses of SARS-CoV-2 still play a vital role in preventing and controlling the spread of infectious disease.

Since the outbreak of the COVID-19, virus detection methods have been widely studied and applied in practice. It can be roughly divided into two categories: nucleic acid testing and antigen testing. Real-time reverse transcription-polymerase chain reaction (RT-PCR) has been

widely recognized as the gold standard for SARS-CoV-2 nucleic acid testing due to its accuracy and specificity (Bwire et al., 2021). However, RT-PCR involves nucleic acid extraction and amplification processes, which require specialized laboratories and technical expertise, resulting in a turnaround time of over 2 h (Koehler et al., 2021). Two notable new methods have been introduced for nucleic acids testing: loop-mediated isothermal amplification (LAMP) (Ganguli et al., 2021; Zhu et al., 2020) and CRISPR-based assays (Li et al., 2022; Ma et al., 2022). These methods largely decreased detection time but exhibit less sensitivity than PCR technology.

Direct antigen (N-protein, S-protein or whole virion) tests are also successful and have been commonly used for the diagnosis of COVID-19

(Lerner et al., 2020; Peeling et al., 2020). Lateral-flow assay (LFAs) of antigen stands out as simple, rapid, and cost-effective POC diagnostic methods. Many have been commercialized for point-of-care or home-use. Some LFAs hold the potential for wide-scale population screening (Taleghani and Taghipour, 2021). However, so far, none of the antigen detecting methods have achieved the same level of sensitivity and quantitation capability as RT-PCR (Van Elslande et al., 2020; Yakoh et al., 2021). So, unlike nucleic acid testing, antigen testing only detects positivity about a week after infection, resulting in delayed diagnosis.

The field-effect transistor (FET) sensor is a type of electronic device that utilizes the electrical properties of a semiconductor to detect and measure changes of charged environment induced by the binding of analyst on the sensing surface (Fan et al., 2023; Heller et al., 2008). The sensor operates based on the principle of the field effect, where a small potential alteration may induce a pronounced change of channel current (He et al., 2012). FET-based biosensors have several advantages, including high sensitivity, real-time measurements and label-free detection (Nakatsuka et al., 2018; Seo et al., 2020). Nevertheless, silicon-based sensors are limited by low signal conversion efficiency and poor detection performance because of their bulk channel (10^2–10^4 nm) (Chia et al., 2021). Researchers have been exploring alternative semiconductor materials with supreme physical and electrical properties. Among these alternatives, aluminum gallium nitride/gallium nitride (AlGaN/GaN heterogeneous) is regarded as a very promising candidate. This material possesses unique electrical properties, including the spontaneous polarization between the AlGaN and GaN layers and piezoelectric effect occurring in the AlGaN layer. These characteristics give rise to a high density and mobility of the two-dimensional electron gas (2DEG) at the interface of the heterostructure (Parker, 2021). Unlike conventional FETs, the 2DEG in AlGaN/GaN high electron mobility transistor (HEMT) is confined in a narrow quantum well, serving as a two-dimensional (2D) channel instead of a three-dimensional (3D) channel. This design exhibits superior sensing characteristics, as the gate/surface potential can uniformly and easily control the carriers in the 2DEG channel and is very sensitive to the changes in surface charges (Huang et al., 2013; Sun et al., 2019, 2020) When used for the analysis of biomolecules, AlGaN/GaN-based HEMT sensors also exhibit excellent chemical stability and biological compatibility (Anderson et al., 2013; Liu et al., 2023). Moreover, mass manufacturing of AlGaN/GaN HEMT with the standard microelectronic processes supports the cost-effective, high-consistency and easy integration of GaN-based biosensors for a wide range of applications.

In this study, we first propose an AlGaN/GaN HEMT based biosensor and evaluate the performance of this biosensor by detecting SARS-CoV-2 spike proteins, SARS-CoV-2 pseudoviruses and SARS-CoV-2 ΔN virions. We have demonstrated that this sensor sensitively and real-time captures the changes in the AlGaN/GaN heterostructure channel, induced by the binding events on the sensing surface, and resulted in a detection limit of 10^{-22} M for spike proteins and single particle sensitivity for virions within 10 min. Moreover, the excellent specificity and stability of the biosensors is also verified for reliable detection.

2. Materials and methods

2.1. Materials

N-(3-(dimethylamino)propyl)–N′-ethyl-carbodiimide hydrochloride (EDC), N-hydroxysuccinimide (NHS), 11-Mercaptoundecanoic (11-MUA), Bovine serum albumin (BSA), phosphate buffered saline (PBS) were all purchased from Sigma-Aldrich Co. SARS-CoV-2 spike S1+S2 ectodomain (ECD) protein and anti-SARS-CoV-2 spike protein antibody (anti-spike protein antibody) were purchased from Sino Biological Co. SARS-CoV-2 pseudoviruses with EGFP/Luciferase tag were purchased from Obio Biotech Co. The concentration of pseudoviruses was determined by the manufacturer using quantitative polymerase chain reaction (qPCR).

The AlGaN/GaN heterostructure epilayers were grown on a <111> silicon wafer, 100 mm in diameter and 675 μm thick, using Metal-organic Chemical Vapor Deposition (MOCVD). The epitaxial structure consisted of an undoped GaN buffer layer (500 nm), followed by an AlN interlayer (0.8 nm), an undoped $Al_{0.25}Ga_{0.75}N$ barrier layer (24 nm), and a 2.5 nm GaN cap layer.

2.2. Fabrication of AlGaN/GaN HEMT

The fabrication process started with a mesa etching step to define the active area. Then, Ti/Al/Ti/Au (20/110/40/50 nm) metal contacts were evaporated, followed by a rapid thermal anneal at 870 °C for 45 s under N_2 ambient. A 200-nm plasma enhanced chemical vapor deposition (PECVD) SiO_2 layer was then deposited for isolation from the interconnect layer. To establish metal interconnects, a Ti/Au/Ti (10/300/10 nm) layer stack was prepared by evaporation. The topside of the wafer was passivated with a 100/200 nm PECVD SiO_2/Si_3N_4 layer. The SiO_2/Si_3N_4 layer was etched by inductively coupled plasma (ICP). followed by treatment in a buffered oxide etchant (BOE)solution to expose the contact pads and gate windows. Then, a Ti/Au (2/10 nm) layer was evaporated and patterned on the 600 μm × 600 μm gate area. A 6 μm Bis-BenzoCycloButene (BCB) was encapsulated on the wafer and patterned by a photo-lithography process. Finally, the wafer was diced and packaged on the printed circuit board (PCB).

2.3. Biofunctionalization of HEMT sensors

To get a clean gate electrode surface, the Au electrode was treated with piranha solution (H_2O_2:H_2SO_4 = 3:7) for 10 min, followed by several washes with ethanol and dried by N_2. The cleaned gold electrode was then immersed in the 11-mercaptoundecanoic acid (11-MUA, 50 mM) solution in dark overnight to introduce carboxylic groups. These groups were activated by incubating the electrode in a mixed solution of EDC (20 mg/mL) and NHS (10 mg/mL) for 0.5 h at room temperature. The electrode was then rinsed several times with ethanol and DI water to remove extra residues.

The functionalized Au electrode was immersed in a solution of anti-SARS-CoV-2 spike protein antibodies (0.2 mg/mL in 10 mM PBS solution) for 2 h. Afterward, the gates were treated with MEA (1 M, in 10 mM PBS solution) for 0.5 h to eliminate the unreacted carboxylic groups. BSA solution (0.1 mg/mL) was further added for 0.5 h to block the remaining non-specific binding sites on the Au electrode. Finally, a Polydimethylsiloxane (PDMS) opened well with a width of 1.5 cm was placed on the top of the AlGaN/GaN HEMT biosensor to hold the sample solutions.

2.4. Characterization of HEMT sensors

AFM (Dimension FastscanBio, Bruker) was employed to measure the surface topography of Au before and after functionalization. The binding component was measured by XPS (ESCALAB 250Xi, Thermo Fisher). Surface plasmon resonance (SPR) was utilized to assess the construct of the biolayer. The optical signal was measured as the shift of the response unit (RU) at the wavelength of 670 nm. Protein accumulation on the chip was calculated as (*Handbook of Surface Plasmon Resonance*, 2017):

$$1000 \, RU = 100 \, ng/cm^2$$

2.5. Device measurement

Electrical performance measurement was conducted by a semiconductor digital sourcemeter (2614 B, Keithley Instruments, OH). To assess the ionic strength, transfer characteristics were measured in various ionic strength solutions, including de-ionized water, 10 μM PBS, 100 μM PBS, 1000 μM PBS with $V_{GS} = -2$ to -1 V and $V_{DS} = 0.5$ V. The SARS-CoV-2 spike protein, pseudoviruses and SARS-CoV-2 N virions at a
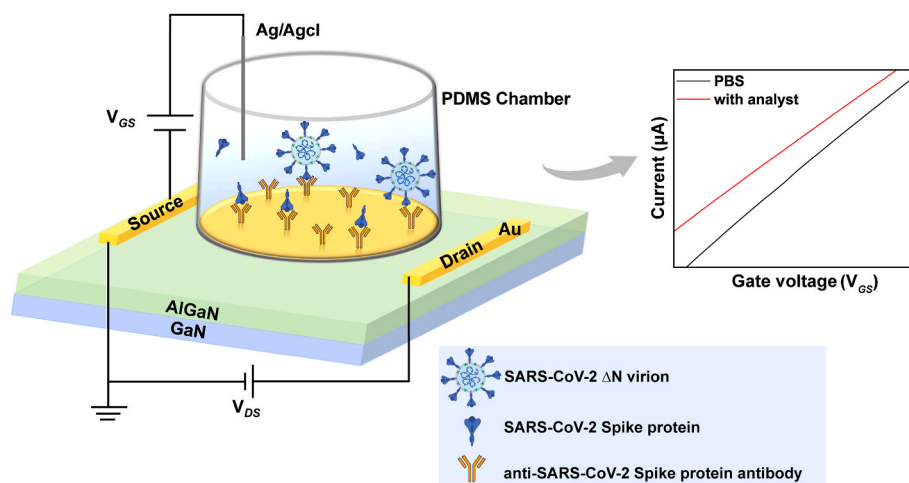
Fig. 1. Schematic diagram of the AlGaN/GaN heterostructure-based biosensor.
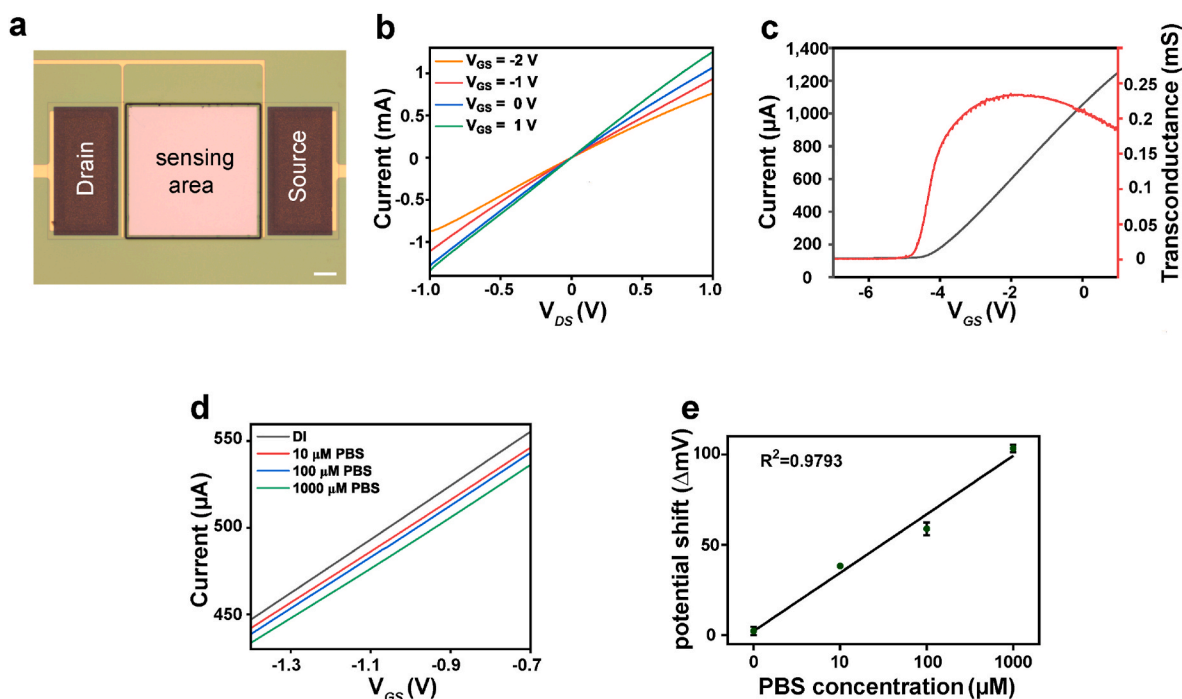

Fig. 2. Electrical property of HEMT biosensor. (a) Optical micrograph of the fabricated AlGaN/GaN HEMT biosensors (scale bar, 100 μm). (b) Output curve of sensors in various gate voltage. (c) Transfer curve of the AlGaN/GaN HEMT biosensor for $V_{DS} = 0.5$ V and associate transconductance. (d) Transfer characteristics measured after exposing the AlGaN/GaN HEMT biosensor to PBS solution with increasing concentration from 10 μM to 1 mM. (e) Potential shift plotted as a function of PBS concentration. Each data point represents the mean value and standard deviation, acquired from three independent measurements.

specific concentration were prepared by serially diluting using 0.01x PBS, similar to the control group. To avoid possible disturbance caused by sample replenishment, we took out 90 μL from PDMS well and injected 90 μL of analyte solution to keep the total volume at 900 μL. An Ag/AgCl electrode was set to provide liquid-gate voltage through the analyte solution. Transfer characteristics were taken with $V_{GS} = -2$ to 0 V and $V_{DS} = 0.5$ V, and the relative change of the gate voltage ΔV_G was calculated after the antigen-antibody reaction.

2.6. Production of SARS-CoV-2 ΔN virions

The production of SARS-CoV-2 ΔN virions at BSL-2 laboratory using nucleocapsid (N)-based genetic complementation system was described previously (Ju et al., 2021). Briefly, cDNAs of SARS-CoV-2 ΔN were

synthesized. The N gene was replaced with the gene encoding GFP. RNA transcripts were generated using the mMESSAGE mMACHINE T7 Transcription Kit (ThermoFisher Scientific) and transfected into Caco-2-N cells by electroporation. The produced SARS-CoV-2 ΔN virions were titrated following Reed & Muench method (Lei et al., 2021).

3. Result and discussion

3.1. Electrical property of HEMT biosensor

Fig. 1 illustrates the schematic of AlGaN/GaN heterostructure biosensor investigated in this study. The biosensor is a liquid-gated AlGaN/GaN HEMT biosensor with an Ag/AgCl reference electrode inserted in the PDMS well, serving as the gate electrode. The fabricated
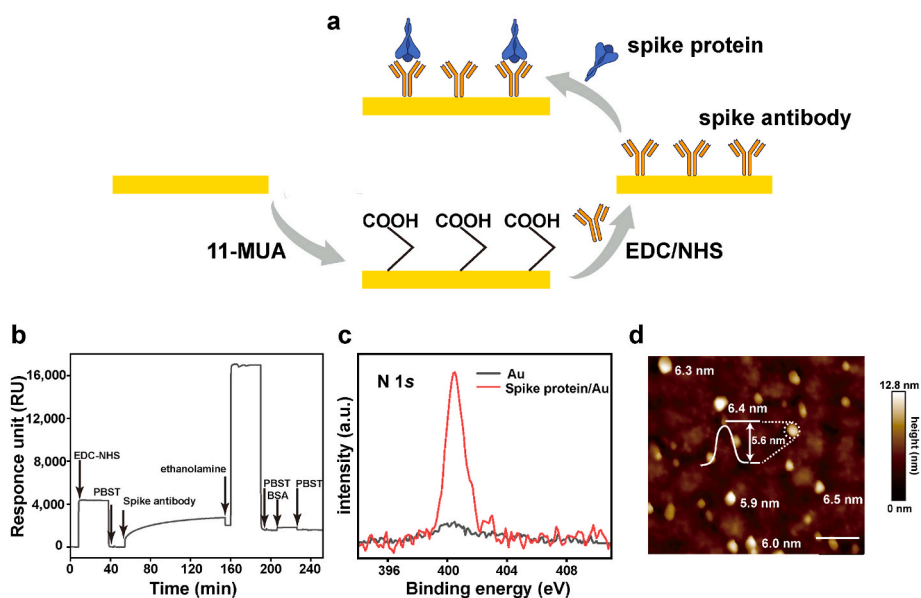
Fig. 3. Characteristics of the biofunctionalization of AlGaN/GaN HEMT biosensor. (a) Schematic illustration of the anti-spike protein antibodies immobilized on the HEMT biosensor. (b) Sensogram of the immobilization of spike antibody on the Au surface pre-modified with the 11-MUA by SPR. (c) AFM image of Au gate modified with anti-spike protein antibodies. (d) XPS N 1s peak of Au gate after bio-functionalization (scale bar, 100 nm).

biosensors are displayed in Fig. 2a, the scheme of fabrication was shown in Fig. S1. To evaluate the electrical properties of AlGaN/GaN HEMT biosensor, it was subjected to measurements using a drain-source voltage (V_{DS}) ranging from -1 V to 1 V and a gate voltage (V_{GS}) ranging from -2 V to 1 V in PBS. As shown in Fig. 2b, the biosensor exhibits the capability to effectively gate control the intrinsic channel. The transfer characteristic of the pristine HEMT biosensor is displayed in Fig. 2c, showing a maximum transconductance of 0.23 mS at $V_{DS} = 0.5$ V. These results suggest that the AlGaN/GaN HEMT biosensor operates within the linear region under bias conditions, aligning with the typical FET model (Chu et al., 2017).

Moreover, we conducted measurements on the AlGaN/GaN HEMT biosensor to assess its response to solutions of different ionic strength solutions. Fig. 2d shows the transfer characteristic of the device. As the concentration of PBS increases, a consecutive right-shift of V_{GS} and a corresponding signal change of 95 mV are observed across the test range (Fig. 2e). These results reveal that the biosensor has the ability to detect alterations in the sensing surface potential with a good linear relationship. Considering the notable shift observed around 100 μM PBS, we selected 100 μM for the subsequent detection.

3.2. Biofunctionalization of AlGaN/GaN HEMT biosensor with anti-SARS-CoV-2 spike protein antibodies

The biofunctionalization of sensor suface plays a crucial role in biomolecule detection (Fig. 3a). The recognition elements were covalently bonded to 11-mercaptoundecanoic that was previously modified on the sensing area and activated through Sulfo-NHS chemistry. The sensing surface was then treated with MEA to eliminate unreacted carboxylic groups, followed by the addition of BSA to block nonspecific binding sites. To validate the successful coupling of anti-spike protein antibodies to the gold surface of sensing surface, surface plasmon resonance (SPR) was employed to monitor the various steps of bio-functionalization process (Fig. 3b). The bare Au SPR slide is modified with 11-MUA overnight, and the surface coverage changes occurring as the biolayer deposited on the sensing area were recorded as a function of time as shown in Fig. S2. The SPR results indicated that a coverage of 285 ng/cm^2 for anti-spike protein antibodies. Considering the sensing area is 0.36 mm^2 and the molecular weight of a single anti-spike protein antibody molecule is about 150 kD, we estimated that the total number of active binding sites immobilized on the gate electrode is almost 5.9×10^9 per unit area, and the output and transfer characteristic curve before and after bio-functionalization were shown in Figs. S3–4.
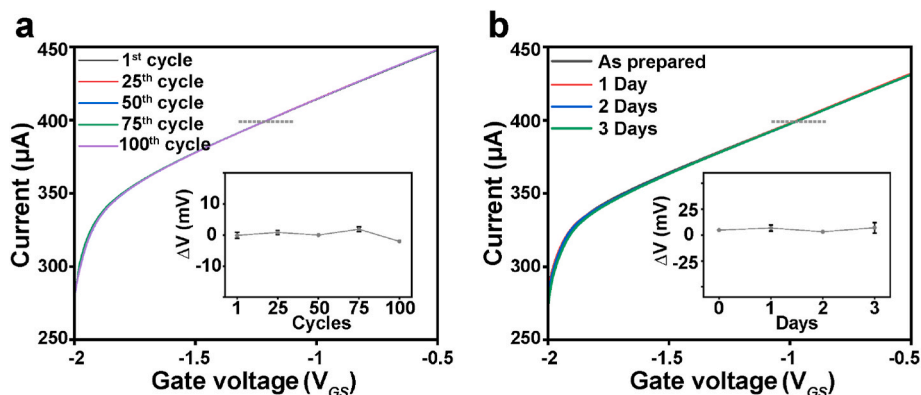

Fig. 4. Stability of AlGaN/GaN HEMT biosensor. (a) stability test of 100 cycles of transfer measurement. (b) Transfer curves of the antibody-modified HEMT biosensor after different periods of storage.
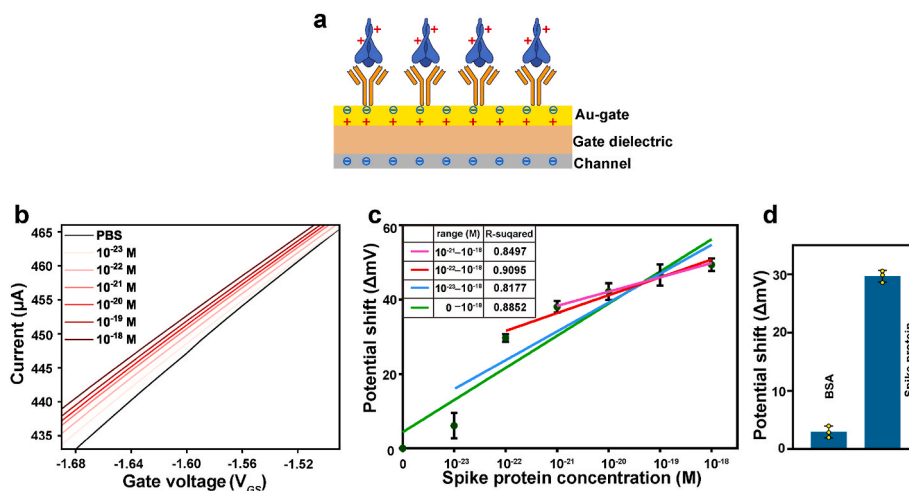
Fig. 5. Detection of SARS-CoV-2 spike proteins with AlGaN/GaN HEMT biosensor. (a) sensing mechanism of HEMT biosensor. (b) transfer characteristics measured after exposing the AlGaN/GaN biosensor to SARS-CoV-2 spike protein with concentration of 10^{-22} M to 10^{-18} M. (c) The potential shift of HEMT biosensor plotted as a function of spike protein concentration. (d) The potential shift of HEMT biosensor measured upon exposure to a 10^{-18} M BSA solution and 10^{-22} M spike protein solution.

The chemical composition of pristine sensing area and sensing area after antibody modification was determined by X-ray photoelectron-spectroscope (XPS). Fig. 3c indicates an appreciate N 1s peak following the anti-spike protein antibody modification, providing evidence of the presence of nitrogen from antibodies bound to the sensing area. Furthermore, atomic force microscopy (AFM) was also employed to confirm the effective modification of anti-spike protein antibodies on the sensing area (Xu et al., 2022). Fig. 3d shows the sensing area is covered with anti-SARS-CoV-2 spike protein antibodies with an average height of 6.12 nm, which is consistent with previous literature (Wu et al., 2020).

Taken together, the results obtained from SPR, AFM and XPS collectively confirm the successful deposition of bio-capturing SAM onto the sensing area, and this highly packed sensing area enables the further detection of spike proteins and virions with high specificity and sensitivity.

3.3. Stability of AlGaN/GaN HEMT biosensor

The stability of biosensors is a crucial requirement for their clinical use. Previous research has shown that Au electrode can be affected when exposed to ionic solutions, leading to unpredictable shifts (Minot et al., 2007). Therefore, in our HEMT biosensor, a uniform passivation layer (SiO_x/SiO_2) was deposited on the drain and source electrode to isolate the electrode from solution. To investigate the stability of the devices, 100 continuous measurement cycles of transfer characteristics were carried out. As shown in Fig. 4a, the HEMT biosensor presents excellent operational stability with negligible performance spread over 100 continuous transfer measurement cycles in pristine. Furthermore, to examine the feasibility of our HEMT biosensor for clinical testing, a long-term test was conducted after the devices were biofunctionalized with anti-spike protein antibodies. Fig. 4b displays the representative transfer curve obtained after varying days of storage. Benefiting from the passivation layer, the value of V_{GS} remains nearly constant even when the HEMT biosensor was immersed in a liquid environment for three days. Consequently, we conclude that our HEMT sensor exhibits excellent stability.

3.4. Detection of SARS-CoV-2 spike protein with AlGaN/GaN HEMT biosensor

To investigate the potential of the HEMT biosensor for the detection

of the SARS-CoV-2, we first employed the HEMT sensor to detect purified spike proteins. The SARS-CoV-2 spike protein was serially diluted to different concentrations in a 0.01x PBS solution, and the solution was then injected into the PDMS well. We measured the transfer characteristic with $V_{GS} = -2$ to 0 V and $V_{DS} = 0.5$ V and the voltage shift was analyzed after 10 min incubation.

In the HEMT biosensor, if the target biomolecules are charged, the captured targets on the sensor surface can result in a change in surface potential (Fig. 5a). The Grahame equation, showing as below, indicates the relationship between surface charge density and surface potential.
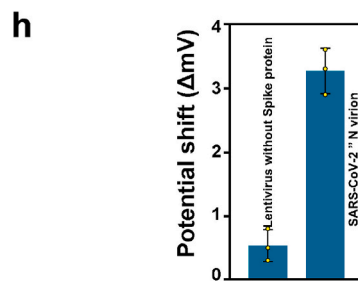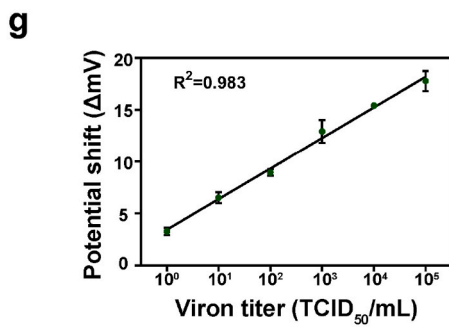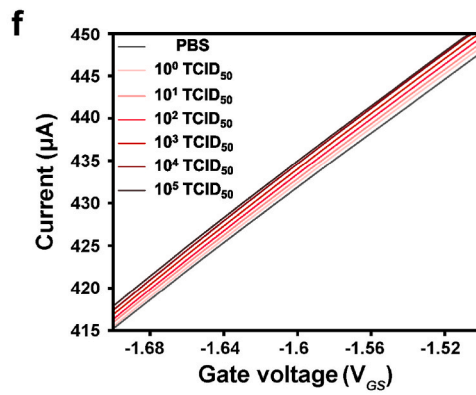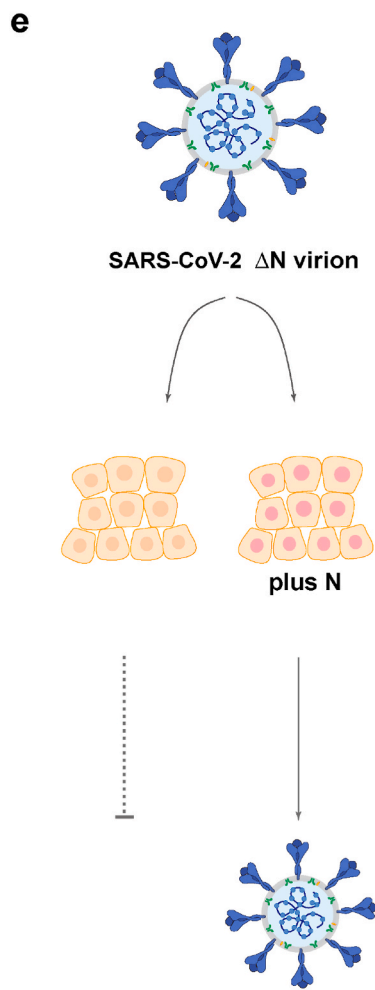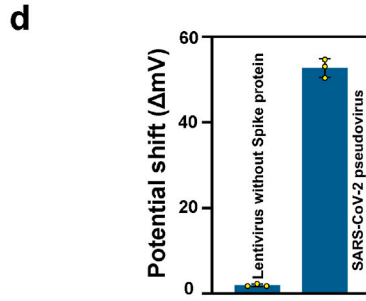
$$\sigma = (8n\varepsilon_r\varepsilon_0 kT)^{\frac{1}{2}} \sinh\left(\frac{ze\psi_0}{2kT}\right) \tag{1}$$

Where σ, ψ_0, ε_r, ε_0 and n are surface charge density, surface potential, relative permittivity, permittivity in vacuum and electrolyte concentration in bulk solution, respectively.

As shown in Fig. 4b, the HEMT biosensor produces a consecutive left shift of V_{GS} with the increase of the concentration of spike proteins and presents a different Coincidence degree in four linear intervals. For the concentration ranging from 10^{-22} M – 10^{-18} M, the R-squared is greater than 0.9, means the fitted regression lines reflect the dose dependent reaction for SARS-CoV-2 spike protein, while others are less than 0.9. It can be observed that there is a significant ΔV_{GS} response around 29.7 mV, even at a concentration as low as 10^{-22} M for the tested spike proteins (Fig. 5c), The detection limit was calculated that the voltage shift can meet the requirement of signal-to-noise (S/N) ratio higher than 3. As a control, the sensor has no obvious response to BSA with concentration of 10^{-18} M (Fig. 5d). These results illustrate the high specificity and sensitivity of the HEMT sensor for the detection of spike protein.

Up to now, several AlGaN/GaN HEMT biosensors have been developed for the sensitive detection of biomolecules. These sensors have achieved a wide detection range of 0.006–148 ng/mL for cardiac troponin I and a detection limit as low as 1 pM for cortisol (Sarangadharan et al., 2018; Woo et al., 2020). Compared with the existing methods, our proposed biosensor presents excellent selectivity and superior sensitivity, which could be explained by the following reasons:

Firstly, the AlGaN/GaN HEMT biosensor proposed in this study leverages the high transconductance provided by the high-electron-mobility 2D channel. The biosensor developed in this work exhibits a transconductance on the order of mS, a significant increase from the typical μS range observed in electrode-gated organic FETs (MacChia

spike-pseudotyped lentiviral partical

b

c

R²=0.9714

d

e

SARS-CoV-2 ΔN virion

plus N

f

g

R²=0.983

h
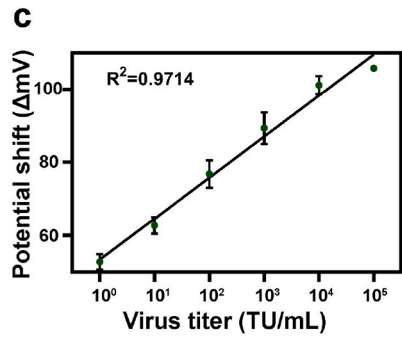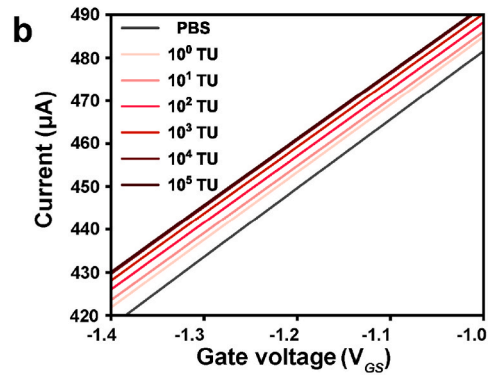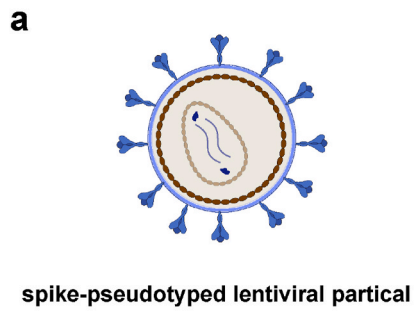
(caption on next page)

Fig. 6. Detection of SARS-CoV-2 pseudoviruses and SARS-CoV-2 ΔN virions with AlGaN/GaN HEMT biosensor. (a) Schematic diagram for the lentivirus-based pseudovirus. (b) Transfer characteristics measured after exposing the AlGaN/GaN biosensor to pseudovirus with increasing titer from 10^0 TU per milliliter to 10^5 TU per milliliter. (c) The potential shift of HEMT biosensor plotted as a function of pseudovirus titer. (d) The potential shift of HEMT biosensor upon 10^5 TU per milliliter of pseudoviruses without spike and 10^0 TU per milliliter of pseudoviruses with spike. (e) Schematic diagram for the preparation of SARS-CoV-2 ΔN virions. SARS-CoV-2 ΔN virion is a gene-deleted virus (loss of N), and it can replicate in host cells only if N proteins are additionally provided, making this system much safer. Therefore, the SARS-CoV-2 ΔN virion can be operated in BSL-2 laboratory. (f) Transfer characteristics measured after exposing the AlGaN/GaN biosensor to SARS-CoV-2 ΔN virions with increasing titer from 10^0 TCID$_{50}$ per milliliter to 10^5 TCID$_{50}$ per milliliter. (g) The potential shift of HEMT biosensor as a function of SARS-CoV-2 ΔN virions titer. (h) The potential shift of HEMT biosensor upon 10^5 TU per milliliter of pseudoviruses without spike and 1 TCID$_{50}$ per milliliter of SARS-CoV-2 ΔN virions.

---

et al., 2020). Theoretically, this elevated transconductance facilitates the amplification of electrostatic signal alterations by a factor of one million (MacChia et al., 2019), thereby enabling the measurement of signal changes instigated by the binding of a singular molecule. Secondly, the large size of transducing interface is also considered a contributing factor to the heightened detection sensitivity. The sensing area of our biosensor is approximately 0.36 mm^2, accommodating a large quantity of biorecognition elements (5.9×10^9 anti-spike protein antibodies per unit area) immobilized on the sensing interface. This expansive sensing area offers a higher geometrical cross section for the binding of analytes with recognition biomolecules, thereby enhancing the ability to detect trace analytes within the sample.

3.5. Detection of SARS-CoV-2 pseudoviruses and SARS-CoV-2 ΔN virions with AlGaN/GaN HEMT biosensor

Up to now, no HEMT sensors have been used for the detection of virions yet. To determine the ability of HEMT sensor for the detection of SARS-CoV-2, both SARS-CoV-2 pseudoviruses and SARS-CoV-2 ΔN virions were employed in our study. The pseudoviruses are constructed based on a lentiviral vector and carry the spike proteins for cell entry and viral infection (Fig. 6a). We first measured the transfer characteristic curves of sensors toward pseudoviruses with series of titters (Fig. 6b). There is linear relationship ($R^2 = 0.9714$) between the potential shift and pseudovirus concentration over the range from 10^0 to 10^5 TU (Transducing Unit) per milliliter (11.23 mV/dec) and the LOD was as low as 1 TU per milliliter (Fig. 6c). As a control, high concentration of the lentivirus without spike protein do not produce obvious response (Fig. S5) (Fig. 6d). While pseudoviruses serve as a useful tool for simulating SARS-CoV-2, the lentivirus vector may elicit distinct responses due to its distinct molecular architecture from that of SARS-CoV-2. Therefore, we tested the SARS-CoV-2 ΔN virions using our proposed sensor. SARS-CoV-2 ΔN virions are engineered particles that possess the full complement of structural proteins and viral genome of SARS-CoV-2 except for the nucleocapsid encoding gene (Fig. 6e). SARS-CoV-2 ΔN virions maintain the intrinsic properties of SARS-CoV-2, while rendering them non-infectious due to the absence of the nucleocapsid protein in cell without nucleocapsid protein. Considering SARS-CoV-2 ΔN virions get replicated only in the cells with expression of nucleocapsid protein, the virions are allowed to be manipulated in BSL-2 laboratories. In this study, the SARS-CoV-2 ΔN virions were titrated following Reed & Muench method. A series concentration of SARS-CoV-2 ΔN virions were injected into the PDMS well, the transfer characteristic curves were measured after 10 min incubation of virions with anti-spike protein antibodies on the sensing gate (Fig. 6f). As we predicted, a consecutive left shift is observed, and Appreciate 3.6 mV is observed upon 1 TCID$_{50}$ per milliliter and remains a perfect linear relationship with 10^0 to 10^5 TCID$_{50}$ per milliliter (2.949 mV/dec) (Fig. 6g). The lentivirus without spike proteins was used as the control group, and there is no strong signal observed even at 10^5 TCID$_{50}$ per milliliter (Fig. S6) (Fig. 6h).

4. Conclusion

This work established a biosensing platform for the label-free, ultra/super sensitive, and specific detection of SARS-CoV-2 using AlGaN/GaN HEMT based immunosensor. Due to the large area interface and high transconductance, this biosensor has demonstrated exceptional capability in detecting SARS-CoV-2 spike proteins at an impressively low concentration of 10^{-22} M and single virion detection limit within 10 min. The biosensor can be fabricated by semiconductor manufacturing at low cost and would be integrated into portable systems. The features validate the potential of AlGaN/GaN HEMT biosensors for POC tests targeting SARS-CoV-2, with significant implications for timely diagnosis of other pathogens and their associated infectious diseases.

CRediT authorship contribution statement

Chenyang Yang: Writing – original draft, Methodology, Investigation, Formal analysis, Data curation, Conceptualization. **Jianwen Sun:** Writing – original draft, Methodology, Investigation, Formal analysis, Data curation, Conceptualization. **Yulong Zhang:** Resources, Methodology, Investigation. **Jingya Tang:** Software, Resources. **Zizheng Liu:** Software, Resources, Formal analysis. **Teng Zhan:** Resources. **Dian-Bing Wang:** Writing – original draft, Methodology, Data curation, Conceptualization. **Guoqi Zhang:** Writing – review & editing, Data curation, Conceptualization. **Zewen Liu:** Writing – review & editing, Data curation, Conceptualization. **Xian-En Zhang:** Writing – review & editing, Writing – original draft, Supervision, Resources, Methodology, Funding acquisition, Data curation, Conceptualization.

Declaration of competing interest

The authors declare that they have no known competing financial interests or personal relationships that could have appeared to influence the work reported in this paper.

Data availability

Data will be made available on request.

Acknowledgements

Appendix A. Supplementary data

Supplementary data to this article can be found online at https://doi.org/10.1016/j.bios.2024.116171.

References

Anderson, T.J., Koehler, A.D., Hobart, K.D., Tadjer, M.J., Feygelson, T.I., Hite, J.K., Pate, B.B., Kub, F.J., Eddy, C.R., 2013. IEEE Electron. Device Lett. 34, 1382–1384. https://doi.org/10.1109/LED.2013.2282968.

Bwire, G.M., Majigo, M.V., Njiro, B.J., Mawazo, A., 2021. J. Med. Virol. 93, 719–725. https://doi.org/10.1002/JMV.26349.

Chia, H.L., Mayorga-Martinez, C.C., Pumera, M., 2021. Adv. Funct. Mater. 31, 2102555 https://doi.org/10.1002/adfm.202102555.

Chu, C.H., Sarangadharan, I., Regmi, A., Chen, Y.W., Hsu, C.P., Chang, W.H., Lee, G.Y., Chyi, J.I., Chen, C.C., Shiesh, S.C., Lee, G. Bin, Wang, Y.L., 2017. Sci. Rep. 7, 1–15. https://doi.org/10.1038/s41598-017-05426-6.

Fan, J., Parr, S., Kang, S., Gupta, M., 2023. Nanoscale 15, 5476–5485. https://doi.org/10.1039/d2nr06485e.

Ganguli, A., Mostafa, A., Berger, J., Lim, J., Araud, E., Baek, J., Stewart De Ramirez, S.A., Baltaji, A., Roth, K., Aamir, M., Aedma, S., Mady, M., Mahajan, P., Sathe, S., Johnson, M., White, K., Kumar, J., Valera, E., Bashir, R., 2021. Anal. Chem. 93, 7797–7807. https://doi.org/10.1021/acs.analchem.0c05170.

Handbook of Surface Plasmon Resonance, 2017. Handbook of Surface Plasmon Resonance. https://doi.org/10.1039/9781788010283.

He, R.X., Lin, P., Liu, Z.K., Zhu, H.W., Zhao, X.Z., Chan, H.L.W., Yan, F., 2012. Nano Lett. 12, 1404–1409. https://doi.org/10.1021/nl2040805.

Heller, I., Janssens, A.M., Männik, J., Minot, E.D., Lemay, S.G., Dekker, C., 2008. Nano Lett. 8, 591–595. https://doi.org/10.1021/nl072996i.

Huang, C.C., Lee, G.Y., Chyi, J.I., Cheng, H.T., Hsu, C.P., Hsu, Y.R., Hsu, C.H., Huang, Y. F., Sun, Y.C., Chen, C.C., Li, S.S., Andrew Yeh, J., Yao, D.J., Ren, F., Wang, Y.L., 2013. Biosens. Bioelectron. 41, 717–722. https://doi.org/10.1016/j.bios.2012.09.066.

Ju, X., Zhu, Y., Wang, Y., Li, J., Zhang, J., Gong, M., Ren, W., Li, S., Zhong, J., Zhang, L., Zhang, Q.C., Zhang, R., Ding, Q., 2021. PLoS Pathog. 17, e1009439 https://doi.org/10.1371/journal.ppat.1009439.

Koehler, P., Bassetti, M., Chakrabarti, A., Chen, S.C.A., Colombo, A.L., Hoenigl, M., Klimko, N., Lass-Flörl, C., Oladele, R.O., Vinh, D.C., Zhu, L.P., Böll, B., Brüggemann, R., Gangneux, J.P., Perfect, J.R., Patterson, T.F., Persigehl, T., Meis, J. F., Ostrosky-Zeichner, L., White, P.L., Verweij, P.E., Cornely, O.A., 2021. Lancet Infect. Dis. 21, e149–e162. https://doi.org/10.1016/S1473-3099(20)30847-1.

Lei, C., Yang, J., Hu, J., Sun, X., 2021. Virol. Sin. https://doi.org/10.1007/s12250-020-00230-5.

Li, Z., Ding, X., Yin, K., Avery, L., Ballesteros, E., Liu, C., 2022. Biosens. Bioelectron. 199 https://doi.org/10.1016/j.bios.2021.113865.

Liu, L., Zhang, H., Xu, R., Zhong, G., Huang, H., Guo, W., Xu, N., Liang, H., 2023. IEEE Electron. Device Lett. 44, 120–123. https://doi.org/10.1109/LED.2022.3225302.

Ma, L., Yin, L., Li, X., Chen, S., Peng, L., Liu, G., Ye, S., Zhang, W., Man, S., 2022. Biosens. Bioelectron. 195 https://doi.org/10.1016/j.bios.2021.113646.

MacChia, E., Picca, R.A., Manoli, K., Di Franco, C., Blasi, D., Sarcina, L., Ditaranto, N., Cioffi, N., Österbacka, R., Scamarcio, G., Torricelli, F., Torsi, L., 2020. Mater. Horiz. https://doi.org/10.1039/c9mh01544b.

MacChia, E., Tiwari, A., Manoli, K., Holzer, B., Ditaranto, N., Picca, R.A., Cioffi, N., Di Franco, C., Scamarcio, G., Palazzo, G., Torsi, L., 2019. Chem. Mater. 31 https://doi.org/10.1021/acs.chemmater.8b04414.

Nakatsuka, N., Yang, K.A., Abendroth, J.M., Cheung, K.M., Xu, X., Yang, H., Zhao, C., Zhu, B., Rim, Y.S., Yang, Y., Weiss, P.S., Stojanović, M.N., Andrews, A.M., 2018. Science 1979 (362), 319–324. https://doi.org/10.1126/science.aao675.

Parker, M., 2021, 2021 Nature Electronics 4 (12 4), 858. https://doi.org/10.1038/s41928-021-00698-3.

Sarangadharan, I., Regmi, A., Chen, Y.W., Hsu, C.P., Chen, P. chi, Chang, W.H., Lee, G.Y., Chyi, J.I., Shiesh, S.C., Lee, G. Bin, Wang, Y.L., 2018. Biosens. Bioelectron. 100, 282–289. https://doi.org/10.1016/j.bios.2017.09.018.

Seo, G., Lee, G., Kim, M.J., Baek, S.H., Choi, M., Ku, K.B., Lee, C.S., Jun, S., Park, D., Kim, H.G., Kim, S.J., Lee, J.O., Kim, B.T., Park, E.C., Kim, S. Il, 2020. ACS Nano 14, 5135–5142. https://doi.org/10.1021/acsnano.0c02823.

Sun, J., Sokolovskij, R., Iervolino, E., Liu, Z., Sarro, P.M., Zhang, G., 2019. J. Microelectromech. Syst. 28, 997–1004. https://doi.org/10.1109/JMEMS.2019.2943403.

Sun, J., Zhang, S., Zhan, T., Liu, Z., Wang, J., Yi, X., Li, J., Sarro, P.M., Zhang, G., 2020. J Mater Chem C Mater 8, 5409–5416. https://doi.org/10.1039/d0tc00553c.

Taleghani, N., Taghipour, F., 2021. Biosens. Bioelectron. 174, 112830 https://doi.org/10.1016/J.BIOS.2020.112830.

Van Elslande, J., Houben, E., Depypere, M., Brackenier, A., Desmet, S., André, E., Van Ranst, M., Lagrou, K., Vermeersch, P., 2020. Clin. Microbiol. Infection 26, 1082–1087. https://doi.org/10.1016/j.cmi.2020.05.023.

Woo, K., Kang, W., Lee, K., Lee, P., Kim, Y., Yoon, T.S., Cho, C.Y., Park, K.H., Ha, M.W., Lee, H.H., 2020. Biosens. Bioelectron. 159 https://doi.org/10.1016/j.bios.2020.112186.

Wu, Y., Li, C., Xia, S., Tian, X., Kong, Y., Wang, Z., Gu, C., Zhang, R., Tu, C., Xie, Y., Yang, Z., Lu, L., Jiang, S., Ying, T., 2020. Cell Host Microbe 27, 891–898.e5. https://doi.org/10.1016/j.chom.2020.04.023.

Xu, L., Ramadan, S., Rosa, B.G., Zhang, Y., Yin, T., Torres, E., Shaforost, O., Panagiotopoulos, A., Li, B., Kerherve, G., Kim, D.K., Mattevi, C., Jiao, L.R., Petrov, P. K., Klein, N., 2022. Sensors and Diagnostics 1, 719–730. https://doi.org/10.1039/d2sd00076h.

Yakoh, A., Pimpitak, U., Rengpipat, S., Hirankarn, N., Chailapakul, O., Chaiyo, S., 2021. Biosens. Bioelectron. 176, 112912 https://doi.org/10.1016/j.bios.2020.112912.

Zhu, X., Wang, X., Han, L., Chen, T., Wang, L., Li, H., Li, S., He, L., Fu, X., Chen, S., Xing, M., Chen, H., Wang, Y., 2020. Biosens. Bioelectron. 166, 112437 https://doi.org/10.1016/j.bios.2020.112437.